INCORPORATING TOPOLOGICAL DERIVATIVES INTO SHAPE DERIVATIVES BASED LEVEL SET METHODS

LIN HE*, CHIU-YEN KAO†, AND STANLEY OSHER *‡

Abstract. Shape derivatives and topological derivatives have been incorporated with level set methods to investigate shape optimization problems. The shape derivative measures the sensitivity of boundary perturbations while the topological derivative measures the sensitivity of creating a small hole in the interior domain. The combination of these two derivatives yields an efficient algorithm which has more flexibility in shape changing and may escape from local optimal. Examples on finding the optimal shapes for maximal band gaps in photonic crystal and acoustic drum problems are demonstrated.

Key words. Shape Derivatives, Topological Derivatives, Level Set Methods, Shape Optimization, Structural Design.

1. Introduction. Shape optimization arises in many different fields, such as mechanical design and shape reconstruction. It can be generally described as a problem of finding the optimal shapes in a certain sense with certain constraints. One of the well-known problems is to find the shape of a bubble which minimize the surface tension or surface area with a fixed volume. The answer is a sphere. Nowadays shape optimization problems with P.D.E. constraints are under extensive study.

One of the difficulties in shape optimization problems is that the topology of the optimal shape is unknown. Developing numerical techniques which can handle topology changes becomes essential for shape optimization problems. The level set method introduced in [15] has been well known for handling topology changes, such as breaking one component into two, merging two components into one and forming sharp corners. Therefore it has been used naturally to study shape optimization problems. Instead of using the physically driven velocity, the level set method typically moves the surfaces by the gradient flow of an energy functional. Previously this gradient flow was computed based on shape derivatives. These approaches based on shape sensitivity include the boundary design of elastic structures in [16], the shape design for drums having certain properties on frequencies in [14] and the shape design for photonic crystals having maximum band gaps in [11].

However, as pointed out in [2, 1], the level set approach based on the shape sensitivity may get stuck at shapes with fewer holes than the optimal geometry in some applications to structure designs. To address this issue, Burger, Hackl and Ring proposed in [5] a modified level set method that includes the topological derivative. This derivative measures the influence of creating a small hole in the interior domain. But in their work, they only applied this new approach to a rather simple example: the minimization of a least squares functional. Thus the main purpose of our paper is to generalize their approach to any objective functional by assuming some continuity conditions of the objective functional.

The remainder of the paper is organized as follows: In Section 2 and Section 3, the shape derivative and the topological derivative are introduced respectively. In

*UCLA Mathematics Department, Box 951555, Los Angeles, CA 90095-1555, U.S.A. ({helin, sjo }@math.ucla.edu)

†Institute for Mathematics and its Applications, 400 Lind Hall, 207 Church St. Minneapolis, MN 55455, U.S.A. kao@ima.umn.edu

‡This research is partially supported by NSF grants DMS- 0312222, ACI- 0321917 and DMI-0327077.

Section 4, the level set method is used to evolve the shape based on shape derivative and/or topological derivative. In Section 5, we show the numerical results for the shape design of drums and photonic crystals. We conclude with an appendix.

2. Shape Derivatives. Shape derivatives measure the sensitivity of boundary perturbations. In the framework of Murat-Simon [12, 18], it is defined as the following. Let $\Omega \in D \subset R^N$ be a reference domain. Consider the perturbation under the map $\theta \in W^{1,\infty}(R^N, R^N)$ s.t. $||\theta||_{W^{1,\infty}} < 1$:

$$\Omega_\theta = (I + \theta)\Omega,$$

where I is the identity map. The set Ω_θ is defined as

$$\Omega_\theta = \{x + \theta(x) \,|\, x \in \Omega\}.$$

The shape derivative of an objective shape functional, $\mathcal{F} : R^N \to R$, at Ω is defined as the Frechet differential of $\theta \to \mathcal{F}(\Omega_\theta)$ at 0. θ can be viewed as a vector field advecting the reference domain Ω. The shape derivative $d_S\mathcal{F}(\Omega)(\theta)$ depends only on $\theta \cdot n$ on the boundary $\partial\Omega$ because the shape of Ω does not change at all if θ is lying on the tangential direction of the domain Ω.

For an objective functional that is the integral on the volume of Ω or along the boundary of Ω, the following formula can be easily obtained. If Ω is a smooth bounded open set, $f(x) \in W^{1,1}(R^N)$, and

$$\mathcal{F}(\Omega) = \int_\Omega f(x)dx,$$

the shape derivative is

$$d_S\mathcal{F}(\Omega)(\theta) = \int_\Omega \nabla \cdot (\theta(x)f(x)) = \int_{\partial\Omega} \theta(x) \cdot n(x)f(x)ds. \tag{2.1}$$

If Ω is a smooth bounded open set, $f(x) \in W^{2,1}(R^N)$, and

$$\mathcal{F}(\Omega) = \int_{\partial\Omega} f(x)dx,$$

the shape derivative is

$$d_S\mathcal{F}(\Omega)(\theta) = \int_{\partial\Omega} \theta(x) \cdot n(x)(\frac{\partial f}{\partial n} + Hf)ds, \tag{2.2}$$

where H is the mean curvature of $\partial\Omega$ defined by $H = \nabla \cdot n$. These two formulas indicate that the shape derivative depends only on the boundary when the objective functional is a volume integral and the curvature plays a role when the objective functional is a surface integral.

After the shape derivative is computed, the gradient flow can be chosen to optimize the objective functional. Suppose the shape derivative is

$$d_S\mathcal{F}(\Omega)(\theta) = \int_{\partial\Omega} \theta(x) \cdot n(x)W(\Omega)(x)ds, \tag{2.3}$$

to maximize the objective functional $\mathcal{F}(\Omega)$, we choose the gradient flow as

$$\theta(x) = W(\Omega)(x)n(x).$$

This means that the normal velocity of the shape is $W(\Omega)(x)$. When we use the zero level set of function ϕ to represent the boundary of Ω, the motion under the normal velocity $W(\Omega)(x)$ is simply

$$\phi_t + W(\Omega)(x)|\nabla\phi| = 0. \tag{2.4}$$

Notice that the shape derivative in (2.3) is only defined on the boundary $\partial\Omega$, however under the level set framework it has to be defined on the whole domain D. In the case that the shape derivative functional is originally defined on D, for example, the shape derivative from (2.1) and (2.2), we can just naturally extend it to D (cf. [14]). There are alternative means to extend the normal velocity $W(\Omega)(x)$ on the zero level set to D, such as the method outlined in [6, 20]. Here we only consider the first case.

3. Topological Derivatives. While the shape derivative is defined on local perturbations of the boundary of the domain Ω, the topological derivative measures the influence of creating small holes at a certain point. The idea of the topological derivative is to create a small ball $B_{\rho,x}$ with center x and radius ρ inside/outside the domain Ω and then consider the variation of the objective functional $\mathcal{F}$ with respect to the volume of this small ball. For $x \in \overline{\Omega}$, the topological derivative $d_{\mathcal{T}}\mathcal{F}(\Omega)(x)$ is defined as the limit (if it exists)

$$d_{\mathcal{T}}\mathcal{F}(\Omega)(x) := \lim_{\rho\to 0} \frac{\mathcal{F}(\Omega_{\rho,x}) - \mathcal{F}(\Omega)}{|B_{\rho,x} \bigcap \Omega|}, \tag{3.1}$$

where $\Omega_{\rho,x} = \Omega - \overline{B(\rho, x)}$. This definition is to subtract material at $x \in \overline{\Omega}$. However, in some situations, it's reasonable to add material at $x \in D - \overline{\Omega}$. In that case, the "set-minus" must be replaced by "union" in equation (3.1). For the sake of simplicity, we will only deal with the "set-minus" case and draw conclusions on the "union" case by analogy.

There does exist objective functionals which are not topological differentiable. For example,

$$d_{\mathcal{T}}|\partial\Omega| = \lim_{\rho\to 0} \frac{|\partial B_{\rho,x}|}{|B_{\rho,x}|} \simeq \lim_{\rho\to 0} \frac{\rho^{N-1}}{\rho^N} = \infty.$$

When the topological derivative does exist, by Taylor expansion we naturally have $F(\Omega_{\rho,x}) = F(\Omega) + \pi\rho^2 d_{\mathcal{T}}\mathcal{F}(\Omega)(x) + o(\rho^2)$ (cf. [17]). That shows $F(\Omega_{\rho,x})$ is second-differentiable with zero first derivative at $\rho = 0$. Furthermore we assume that $F(\Omega_{\rho,x}) \in \mathbb{C}^2(\mathbb{R}, \mathbb{R})$ with respect to ρ for small ρ.

The topological derivative is defined on the situation where a small hole is created at some certain point. However from the analytical point of view, we think the change of the topology happens continuously. Thus we can relate it with the shape change. Specifically, for $x \in \overline{\Omega}$, assuming a hole with radius δ is created already, we consider the shape change from $\Omega_{\delta,x}$ to $\Omega_{\rho,x}$, where $0 < \delta < \rho$. And if we let $\delta \to 0$, then this is exactly the definition of the topological derivative.

The shape change from $\Omega_{\delta,x}$ to $\Omega_{\rho,x}$ corresponds to the velocity $\theta = -n$ and $dt = \rho - \delta$. Based on the central difference scheme for any $\mathbb{C}^2(\mathbb{R}, \mathbb{R})$ functional $E(\rho)$:

$$E(\rho) - E(\delta) = (\rho - \delta)E'(\frac{\rho + \delta}{2}) + O((\rho - \delta)^3),$$

and applying the shape derivative given by (2.3), the topological derivative is computed as the following:

$$\lim_{\rho\to 0} \frac{\mathcal{F}(\Omega_{\rho,x}) - \mathcal{F}(\Omega)}{|B_{\rho,x} \bigcap \Omega|} = \lim_{\rho\to 0}\lim_{\delta\to 0} \frac{\mathcal{F}(\Omega_{\rho,x}) - \mathcal{F}(\Omega_{\delta,x})}{|B_{\rho,x} \bigcap (\Omega - \overline{B_{\delta,x}})|}$$

$$
\begin{aligned}
&= \lim_{\rho\to 0}\lim_{\delta\to 0}\frac{(\rho-\delta)\int_{\partial B_{\frac{\delta+\rho}{2},x}} -W(\Omega_{\frac{\delta+\rho}{2},x})(y)\, n\cdot n ds + O((\rho-\delta)^3)}{\pi\rho^2-\pi\delta^2}\\
&= \lim_{\rho\to 0}\lim_{\delta\to 0}\frac{\int_{\partial B_{\frac{\delta+\rho}{2},x}} -W(\Omega_{\frac{\delta+\rho}{2},x})(y)\, ds}{\pi(\delta+\rho)} + \lim_{\rho\to 0}\lim_{\delta\to 0}\frac{O((\rho-\delta)^2)}{\rho+\delta}\\
&= \lim_{\rho\to 0}\frac{\int_{\partial B_{\rho,x}} W(\Omega_{\rho,x})(x) - W(\Omega_{\rho,x})(y)\, ds}{2\pi\rho} - \lim_{\rho\to 0}\frac{\int_{\partial B_{\rho,x}} W(\Omega_{\rho,x})(x)\, ds}{2\pi\rho}\\
&= -\lim_{\rho\to 0} W(\Omega_{\rho,x})(x)\\
&= -W(\Omega)(x).
\end{aligned}
$$

The last second equivalence requires the Lipschitz continuity of $W(\Omega_{\rho,x})(y)$ with respect to y. Furthermore, the last equivalence requires the continuity of $W(\Omega_{\rho,x}(x))$ with respect to ρ at $\rho = 0$. As we mentioned before, it's only by natural extension that $W(\Omega)(y)$ is defined on the interior point $x \in \Omega$. In practice we have to verify the above both requirements before we carry on any further actions. Due to the similarity of our both numerical examples, we will only verify the above assumptions for the photonic crystal case, see Section 5.1.

By similar deduction for the "union" case, we obtain the topological derivative of the objective functional $\mathcal{F}$ based on a domain Ω

$$
d_{\mathcal{T}}\mathcal{F}(\Omega)(x) = \begin{cases} -W(\Omega)(x) & \text{when } x \in \overline{\Omega} \\ W(\Omega)(x) & \text{when } x \in D - \overline{\Omega}. \end{cases} \tag{3.2}
$$

We mark that it might not be easy to compute the shape derivative of the objective functional $\mathcal{F}(\Omega)$. However the purpose of this paper is to incorporate the topological derivative into the standard level set method, which assumes that the information of the shape derivative is known already. For explicit computations of topological derivatives in shape optimization, etc., we refer to [17, 8, 13, 4, 10].

4. Incorporating shape and topological derivatives into the level set method. In some applications to structural design it is observed that the shape derivative based level set method could be trapped in a local optimum with fewer holes than the "real" optimal geometry. Therefore it is necessary to find some additional forces to generate holes. Here we will try to add a term dependent on the topological derivative to the level set equation. Based on the standard level set equation (2.4), the new equation is formulated as

$$
\phi_t + W|\nabla\phi| + \omega G = 0, \tag{4.1}
$$

where ω is a positive parameter which balances the influence of the additional force term G.

In order to maximize the objective functional $\mathcal{F}$, we do the following reasoning to choose the source term G:

- If $\phi(x,t) < 0$ and $d_{\mathcal{T}}\mathcal{F}(\Omega)(x,t) > 0$, then it is favorable to generate a hole at x which means the value of ϕ should increase.
- If $\phi(x,t) < 0$ and $d_{\mathcal{T}}\mathcal{F}(\Omega)(x,t) < 0$, then the value of ϕ should not increase since it is not favorable to generate holes.

- If $\phi(x,t) > 0$ and $d_{\mathcal{T}}\mathcal{F}(\Omega)(x,t) < 0$, then it's not favorable to add material and thus the value of $\phi(x,t)$ should not decrease.
- If $\phi(x,t) > 0$ and $d_{\mathcal{T}}\mathcal{F}(\Omega)(x,t) > 0$, then it's favorable to add material which means the value of ϕ should decrease.

To simplify the study of the movement of the level set towards zero, we assume that this movement is under the influence of the topological derivative only. Then

$$\phi_t = -\omega G.$$

The term $W|\nabla\phi|$ is ignored for the moment. Thus the choice of G will have to satisfy

$$G(x,t)\begin{cases} < 0, & \text{if } \phi(x,t)d_{\mathcal{T}}\mathcal{F}(\Omega)(x,t) < 0 \\ > 0, & \text{if } \phi(x,t)d_{\mathcal{T}}\mathcal{F}(\Omega)(x,t) > 0. \end{cases}$$

Following the work done by Burger et al. in [5], we also choose to use $G(x,t) = \text{sign}(\phi(x,t))d_{\mathcal{T}}\mathcal{F}(\Omega)(x,t)$. The scale of G is dependent on the topological derivative $d_{\mathcal{T}}\mathcal{F}(\Omega)$ only. However the sign of G is dependent on not only $d_{\mathcal{T}}\mathcal{F}(\Omega)$ but also $\text{sign}(\phi)$, which is decided by the location of the point x relative to the zero level set of ϕ. From the deducted expression of the topological derivative (3.2), we obtain $G = W$. Thus the equation (4.1) becomes

$$\phi_t = -W(|\nabla\phi| + \omega). \tag{4.2}$$

The sign of the velocity W decides the movement of ϕ towards or away from the zero level set. Also the speed of this movement is determined by the magnitude of the gradient of ϕ and the extra constant ω. As we can see, when the zero level set is flat or the point is far away from the boundary, the force induced by this magnitude term $|\nabla\phi|$ would be very small. This is when the force generated by ω makes the main contribution to help the movement not get stuck in a local optimum and to expedite the maximization of the cost functional, to finally reach an optimal shape Ω_0 which $\phi(x,t)W(\Omega_0)(x,t) \leq 0$ for any $x \in D$ (For detailed explanation, see the Appendix A or [5]).

In our numerical experiments, we have tried a variation of (4.2) which has the form

$$\phi_t = -W. \tag{4.3}$$

This equation is related to the work [9] done by Gibou and Fedkiw on segmentation problems. The main part of their idea can be simplified as follows: suppose the level set equation is given by $\phi_t = -W$, they update ϕ by the sign of W :

$$\phi = \begin{cases} -1 & \text{if} \quad W > 0 \\ 1 & \text{if} \quad W \leq 0. \end{cases}$$

However, we choose a different algorithm to update ϕ, see Appendix B. Moreover, we can interpret the equation (4.3) as the propagation of ϕ is driven only by the force of topology changes.

5. Numerical Results. To demonstrate the improvements obtained by incorporating the topological derivative in addition to the shape derivative into the standard level set method, we performed numerical experiments on two models. One is to maximize the band gap of photonic crystals (cf. [11]) which involves solving a simplified

Maxwell's equation. The other is to maximize the spectral gap of an inhomogeneous drum with two different densities (cf. [14]) by solving an eigenvalue problem subject to the mass constraint. The extensive numerical work provides compelling evidence that incorporating the topological derivative into the standard level set method is a powerful approach to optimal design.

5.1. The Photonic Crystal Problem. Photonic crystals are periodic structures composed of dielectric material and designed to exhibit band gaps, i.e., range of frequencies in which electromagnetic waves cannot propagate. In [7, 11] and etc, the problem of designing structures with maximal band gaps is considered under the assumption that the structure is composed of "mixtures" of two given dielectric materials. In [7], a existence proof of the solution for a square array of dielectric columns is presented and a generalized gradient ascent algorithm is applied to solve this problem. However in [11], the result by using the level set method (cf. [15]) has shown great improvements in the value of the gaps and the convergence speed.

To focus on the study of maximizing band gaps in photonic crystals, the following conditions are assumed (cf. [7], [11]): the medium is isotropic, the magnetic permeability is constant, and the dielectric function $\epsilon(x)$ is periodic. Applying the Bloch theorem, the simplified Maxwell's equations on the transverse magnetic (TM) field and the transverse electric (TE) field will become:

$$\begin{cases} -\frac{1}{\epsilon(x)}(\nabla + i\alpha)\cdot(\nabla + i\alpha)E_\alpha &= \frac{\omega_{TM}^2}{c^2}E_\alpha, \\ -(\nabla + i\alpha)\cdot\frac{1}{\epsilon(x)}(\nabla + i\alpha)H_\alpha &= \frac{\omega_{TE}^2}{c^2}H_\alpha, \end{cases}$$

where α is a wave number in the irreducible Brillouin zone and the density function

$$\epsilon(x) = \begin{cases} \epsilon_1 & \text{for } x \notin \Omega \\ \epsilon_2 & \text{for } x \in \Omega. \end{cases}$$

Since we only consider the square lattice, the irreducible Brillouin zone is the triangular wedge in the upper-right corner of the first Brillouin zone $K = [-\pi, \pi]^2$, which is inset in both bottom figures in Fig.5.1. The three special points Γ, X, and M correspond respectively to $\alpha = (0, 0)$, $\alpha = (\pi, 0)$, and $\alpha = (\pi, \pi)$.

We solve the following optimization problems:

1. Maximize the band gap in TM: $\mathcal{F}_{\mathcal{TM}}(\Omega) := \sup_{\epsilon(x)}\big(\inf_{\alpha}\omega_{TM}^{n+1} - \sup_{\alpha}\omega_{TM}^{n}\big)$,
2. Maximize the band gap in TE: $\mathcal{F}_{\mathcal{TE}}(\Omega) := \sup_{\epsilon(x)}\big(\inf_{\alpha}\omega_{TE}^{m+1} - \sup_{\alpha}\omega_{TE}^{m}\big)$.

Here we only maximize the band gap in TM case. The shape derivative of $\mathcal{F}_{\mathcal{TM}}$ (cf. [11]) is

$$d_S\mathcal{F}(\Omega)(\theta) = \int_{\partial\Omega} V_{TM}\theta\cdot n\, ds,$$

where

$$\begin{aligned} V_{TM} = \quad & co\left\{-\tfrac{1}{2}(\epsilon_2 - \epsilon_1)\omega_{TM}^{n+1}|u|^2 : u \in \Upsilon_{TM}^{n+1}(\epsilon, \alpha)\right\} \\ & -co\left\{-\tfrac{1}{2}(\epsilon_2 - \epsilon_1)\omega_{TM}^{n}|u|^2 : u \in \Upsilon_{TM}^{n}(\epsilon, \alpha)\right\}, \end{aligned}$$

where Υ_{TM}^n is the span of all eigenfunctions u associated with the eigenvalues ω_{TM}^n and satisfying the normalization $\int_D \epsilon u^2 = 1$.

Based on the work [3] by Ammari and Nedelec, we know that the eigenvalue $\omega^n_{TM}(\Omega_{\rho,x})$ is second-differentiable for small ρ, so does the corresponding eigenvector $u(\Omega_{\rho,x})(y)$. Combining the fact that $u(\Omega_{\rho,x})(y)$ belongs to $C^\infty(D)$, which of course implies Lipschitz continuous, we obtain that the topological derivative equals $-V_{TM}(x)$.

The level set method (cf. [15]) is applied in [11] to represent the interface between two materials with different dielectric constants, i.e.,

$$\epsilon(x) = \begin{cases} \epsilon_1 & \text{for} \quad \{x : \phi(x) < 0\}, \\ \epsilon_2 & \text{for} \quad \{x : \phi(x) > 0\}. \end{cases}$$

And we update the level set function by solving the standard level set equation (2.4), where the velocity W gives the ascent direction to optimize the desired design (cf. [11]). To incorporate the topological derivative, we just need to add a constant ω as in (4.2).

In our numerical simulations, we consider a photonic crystal with a square lattice $D = [-0.5, 0.5] \times [-0.5, 0.5]$ and we use 64×64 mesh grids. For the reason of clarity, a 3×3 array of unit lattice is shown, see the top of Figure 5.1. This figure is the initial dielectric function $\epsilon(x)$, which is used to maximize the band gap between the third and the fourth eigenvalues in TM. The light color indicates the low dielectric constant $\epsilon_2 = 1$ while the dark color indicates the high dielectric constant $\epsilon_1 = 11.4$. The width of crosses is 0.2. The bottom left figure shows the corresponding band structure for the wave vector α along the boundary of the irreducible Brillouin zone of reciprocal lattice. Compared with the initial band structure, the right side band gap structure for the optimal shape has a quite large space between the third and the fourth eigenvalues.

Furthermore, for the above case of maximizing the band gap between ω^3_{TM} and ω^4_{TM}, results by solving equation (4.2) are shown in Figure 5.2 and 5.3. We present the comparison results of four different choices of the topological derivative parameter ω, which varies from 0 to 10. In Figure 5.2, all of them give almost the same optimal shape. However, it only takes 11 steps to reach the optimal shape when $\omega = 10$ (see Figure 5.3, bottom right), while it takes 28 steps for the standard level set method, i.e. $\omega = 0$ (see Figure 5.3, top left). Moreover, for the case of $\omega = 10$, it's at the 4th step that the gap exceeds over 0.15, while it's not until the 20th step for the case of $\omega = 0$. This fact indicates that, in this case the topological derivative takes the main role at the beginning. During the four experiments, the time step dt is always set to satisfy the CFL condition:

$$\frac{dt}{dx}|W|_\infty = 0.5 < 1.0.$$

Figure 5.4 and 5.5 show the evolution of dielectric distribution of optimizing the band gap for the eighth and ninth eigenvalues in TM. A series of pictures are presented in each figure to demonstrate how topology changes along the iteration.

In Figure 5.4, equation (4.2) is solved with $\omega = 100$. The topology changes drastically from the initial shape with $\inf_\alpha \omega^9_{TM} - \sup_\alpha \omega^8_{TM} = -0.1040$ to the result from the third iteration with gap = 0.2012, see top three pictures in Figure 5.4. We notice that since the third iteration the topology has not changed at all even though the optimal band gap 0.4217 at the 25th iteration has doubled itself from 0.2012. We believe that the use of the topological derivative is critical here. Because the "optimal" shape obtained by using same initial shape but with $\omega = 0$ or $\omega = 10$ is

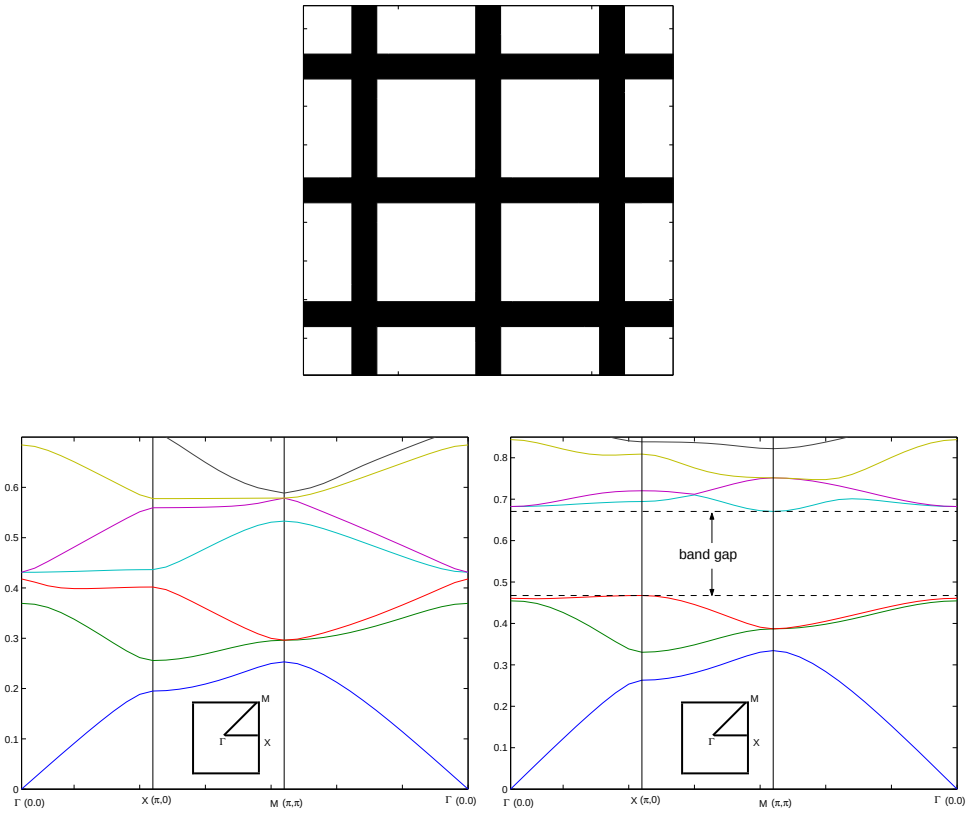

FIG. 5.1. *Top: the initial cross-sectional view of the dielectric distribution; Bottom left: the initial band gap structure; Bottom right: the final band gap structure for maximizing the band gap between* ω^3_{TM} *and* ω^4_{TM}.

obviously stuck at a local optimum, where the band gap of both cases are less than zero.

This belief has been verified again in Figure 5.5, where the level set function is updated via equation (4.3). Thus the propagation of the interface is driven by the force of changing topology only. Again, the change of the topology happens rapidly at the first five iterations and then the topology stays the same while the shape evolves itself to the optimal shape with gap = 0.4323. It shows that topological derivatives are capable of what shape derivatives can do.

The experiment of updating the level set function via equation (4.3) has been tested on different initial shapes with maximizing the band gap for different adjacent eigenvalues. The result of (4.3) is compared with the result of (4.2) with large enough ω and with $\omega = 0$. All start from a same initial shape. Similar behaviors between the solution of(4.3) and (4.2) with large enough ω are observed. One of course, is rapid topology changes at early iterations. In addition, compared with the standard level set method, both have more tendency to surpass a local minimum and both are less dependent on the initial shape. However, there are some issues regarding to the choice of the time step to solve this ODE problem (4.3). For details, please read Appendix B below.

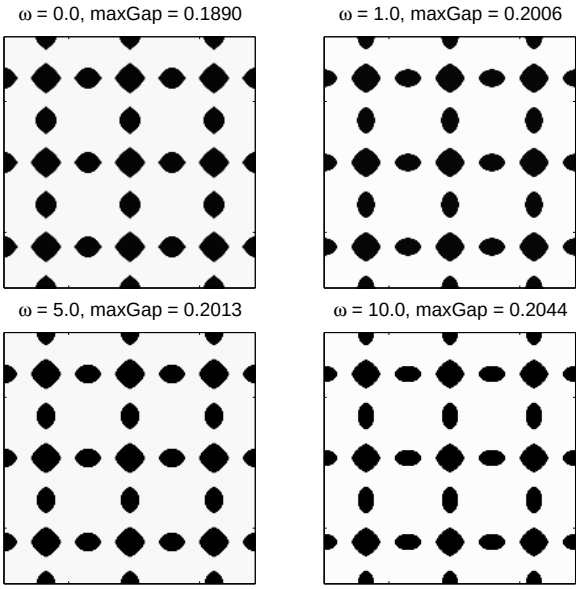

FIG. 5.2. *Comparison results of the dielectric distribution between different choices of ω for maximizing the band gap between ω_{TM}^3 and ω_{TM}^4.*

5.2. The Acoustic Drum Problem. The resonant frequencies of a drum satisfies the eigenvalue problem (cf. [14])

$$\begin{cases} -\Delta u(x) &= \lambda\epsilon(x)u(x) & x \in & D \\ u &= 0 & x \in & \partial D. \end{cases}$$

Let $\Omega \subset\subset D$ be a domain inside D. Suppose that the density $\epsilon(x)$ only takes two values

$$\epsilon(x) = \begin{cases} \epsilon_1 & \text{for} \quad x \notin \Omega \\ \epsilon_2 & \text{for} \quad x \in \Omega, \end{cases}$$

and the mass is a constant which implies

$$\int_\Omega dx = c$$

where c is a constant. By using the Lagrange multiplier method, maximal band gaps between λ_{k+1} and λ_k can be found by maximizing the following objective functional

$$\mathcal{F}(\Omega) = \lambda_{k+1}(\Omega) - \lambda_k(\Omega) + \nu\left(\int_\Omega dx - c\right),$$

where ν is the Lagrange multiplier. The shape derivative of $\mathcal{F}$ is

$$d_S\mathcal{F}(\Omega)(\theta) = \int_{\partial\Omega} (v + \nu)\,\theta \cdot n\, ds,$$

where

$$v(x) = \lambda_{k+1}(\epsilon_2 - \epsilon_1)u_{k+1}^2(x) - \lambda_k(\epsilon_2 - \epsilon_1)u_k^2(x). \tag{5.1}$$

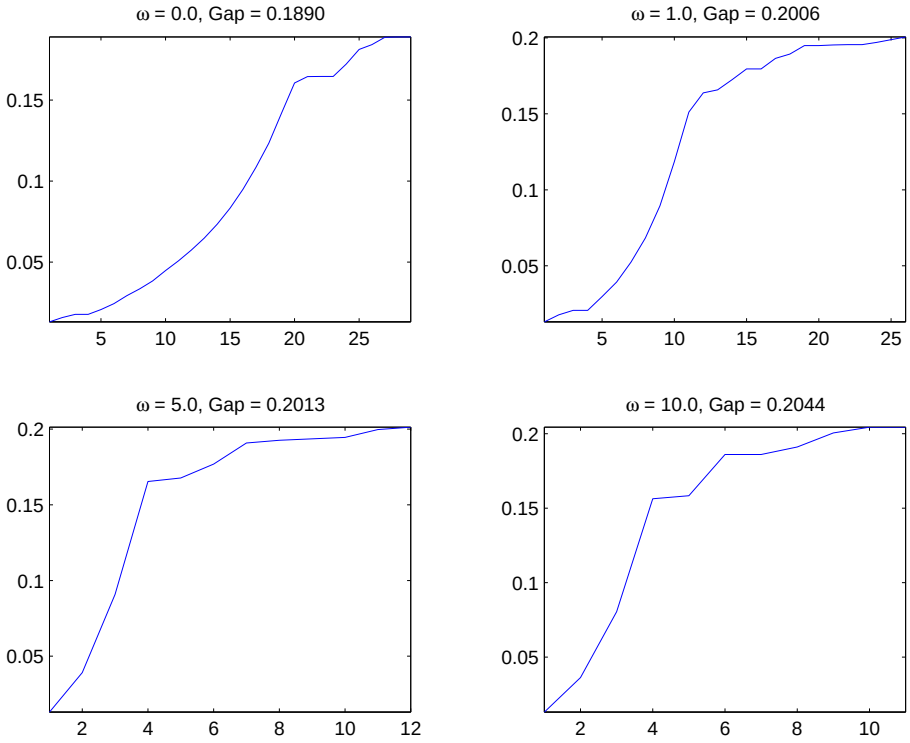

FIG. 5.3. *Comparison results of the band gap vs the iteration between different choices of* ω *for maximizing the band gap between* ω_{TM}^3 *and* ω_{TM}^4.

and

$$\nu = -\frac{\int_D \nabla \cdot v\, n\, dx}{\int_D \nabla \cdot n\, dx} \tag{5.2}$$

is obtained based on the projection approach from the mass constraint. The eigenfunction $u(x)$ satisfies the normalization $\int_D \epsilon u^2(x)\, dx = 1$. We start from an initial guess for ϕ:

$$\epsilon = \begin{cases} \epsilon_1 & \text{for} \quad x \notin \Omega \quad \{x : \phi(x) < 0\} \\ \epsilon_2 & \text{for} \quad x \in \Omega \quad \{x : \phi(x) > 0\}, \end{cases}$$

compute the gradient ascent direction $W = v + \nu$ and evolve ϕ by the standard level set equation (2.4) for one time step. After ϕ is updated, new distribution of density and gradient ascent direction can be computed. This procedure is repeated until the static state is reached. Refer to [14] for detail algorithms. For the approach based on the combination of shape derivative and topological derivative, equation (4.2) is solved with $\omega = 10$.

We show the numerical results based on purely shape derivatives and the combination of shape derivatives and topological derivatives for spectral gap from $\lambda_2 - \lambda_1$ to $\lambda_5 - \lambda_4$. We can clearly see that the algorithms based on two different approaches yield different evolutions. In general, the second approach which is based on combination of shape derivatives and topological derivatives is more flexible on shape changing

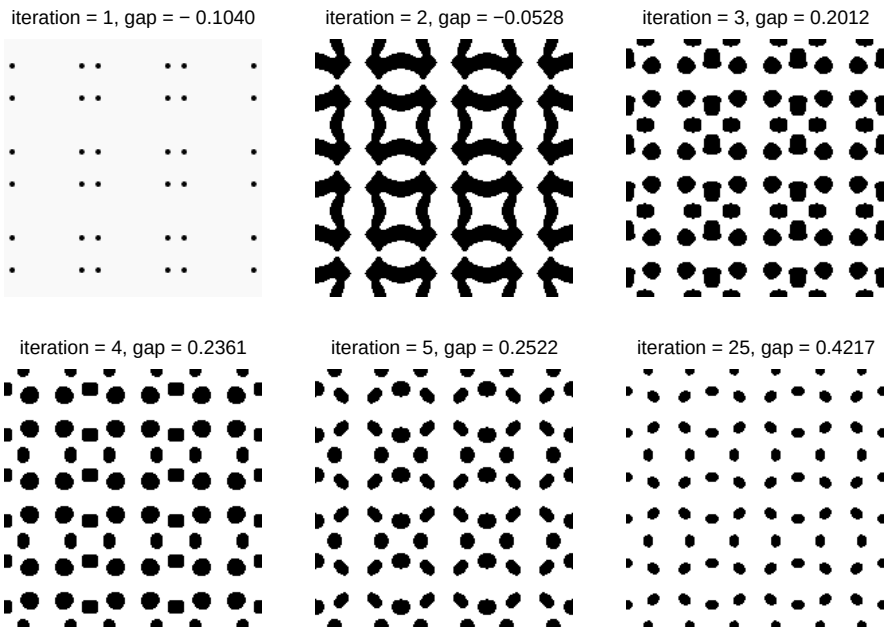

FIG. 5.4. *The evolution of the dielectric distribution by solving* $\phi_t + W(|\nabla\phi| + 100) = 0$ *for maximizing the band gap between* ω^8_{TM} *and* ω^9_{TM}.

because it can easily generate new holes. For optimizing $\lambda_2 - \lambda_1$, the evolutions are pretty much the same for both approaches, see Figure 5.6 and 5.7. However, the second approach reaches static state much faster than the first approach. It takes less than 50 iterations. For optimizing $\lambda_3 - \lambda_2$, the second approach easily creates new holes and also reaches static state faster, see Figure 5.8 and 5.9. For optimizing $\lambda_4 - \lambda_3$, the first approach gets stuck in a local maximum $\lambda_4 - \lambda_3 = 15.2323$ while the second approach obtains a different optimal shape which has a larger gap $\lambda_4 - \lambda_3 = 16.3642$, see Figure 5.10 and 5.11. For optimizing $\lambda_5 - \lambda_4$, it is again the example that both approaches reach same static state but the second approach offers a faster way, see Figure 5.12 and 5.13.

6. Appendix.

6.1. Appendix A. Suppose Ω_0 is the optimal shape given. If there is a point $x \in D$ such that $\phi(x,t)W(x,t) > 0$, then either both of $\phi(x,t)$ and $W(x,t)$ are positive or negative. If both are positive, which means the point $x \in D - \overline{\Omega_0}$ and the topological derivative $d_{\mathcal{T}}\mathcal{F}(\Omega_0)(x,t) = W(x,t) > 0$, then we should add material at x; if both are negative, that means the point $x \in \Omega_0$ and $d_{\mathcal{T}}\mathcal{F}(\Omega_0)(x,t) = -W(x,t) > 0$, then we should create holes at the point x. In either case, the topology has to be changed. That of course, shows Ω_0 is not an optimal shape.

In our experimental results of optimal shape, we observe some points which satisfy $\phi(x,t)W(x,t) > 0$. See points inside the white area but outside the circle in Figure 6.1. They satisfy $\phi(x,t) < 0$ and $W(x,t) < 0$. We consider this area as the diffusion area because the values of W at these points in the area are small.

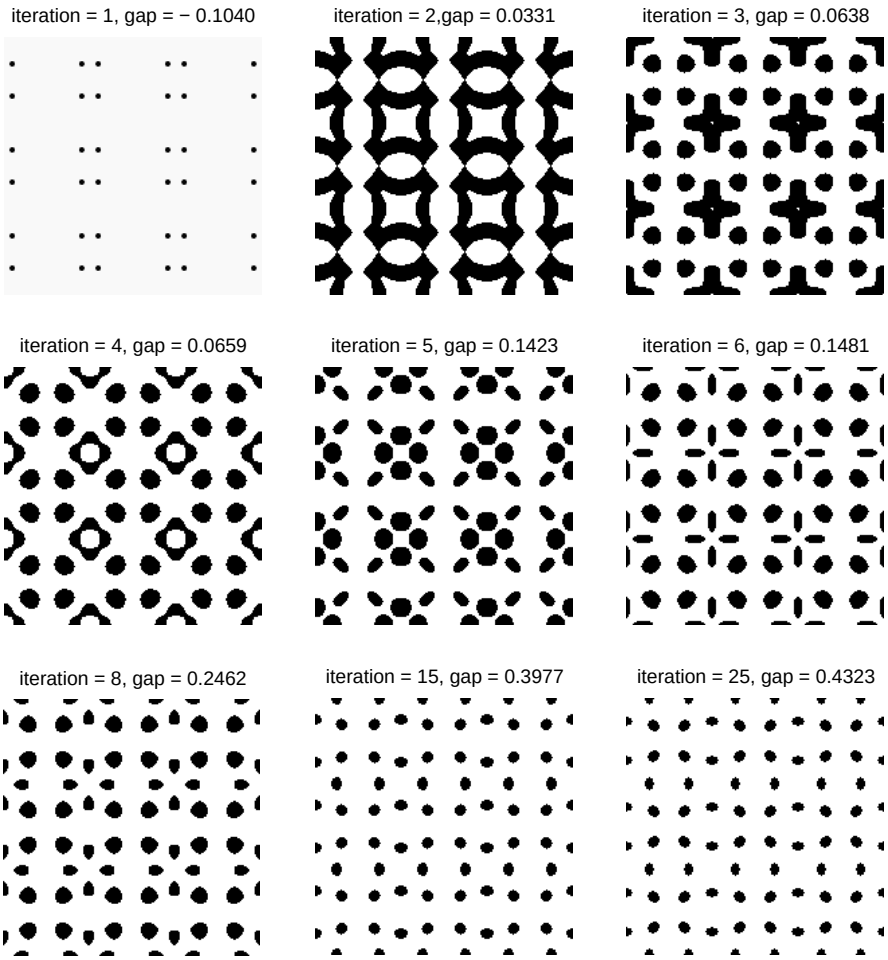

FIG. 5.5. *The evolution of the dielectric distribution by solving* $\phi_t = -W$ *for maximizing the band gap between* ω_{TM}^8 *and* ω_{TM}^9.

6.2. Appendix B. First we denote $T_{i,j}^n = \max(\frac{\phi_{i,j}^n}{W_{i,j}^n}, 0)$, $M = \max_{i,j}\{T_{i,j}^n\}$ and $m = \min_{i,j}\{T_{i,j}^n\}$. Then we let $dt = M$ and take the following steps to update the level set function from ϕ^n to ϕ^{n+1} :

1. While $dt \geq m$, we compute ϕ^{n+1} through $\phi^{n+1} = \phi^n - dt * W^n$; otherwise we stop here which is considered as our optimal shape.
2. Compute the new band gap of dielectric distribution ϵ determined by ϕ^{n+1}. When the new gap is smaller than the old gap, let $dt = \frac{dt}{2}$, go back to step 1.

We state that the purpose of choosing $dt = M$ is to impose an "optimal shape" according to W. However, sometimes the monotonicity of the band gap requires a smaller time step when the band gap is not increasing. This idea of using an energy function as the criterion is related with the work of Song and Chan in [19]. Unfortunately, the above algorithm often needs to go back to step 1 for several times before obtaining a larger new gap. It is very time consuming considering the large computation of eigs() function in Matlab. The problem of choosing an efficient time

step dt would be discussed in future work.

7. Acknowledgements. We thank Samuel Amstutz for helpful comments.

REFERENCES

[1] G. Allaire, F. Jouve, and A. Toader, *Structural optimization using sensitivity analysis and a level-set method*, J. Comput. Phys., 194 (2004), pp. 363–393.

[2] G. Allaire, F. Jouve, and A.-M. Toader, *A leve-set method for shape optimization*, C.R. Acad. Sci. Paris, Ser. I, 334 (2002), pp. 1125–1130.

[3] H. Ammari and J.-C. Nedelec, *Pertubations of eigenvalue problems in electromagnetics*. C.M.A.P. Report 367, 1997.

[4] S. Amstutz, *Sensitivity analysis with respect to a local perturbation of the material property*, Asymptotic Analysis, 49 (2006), pp. 87–108.

[5] M. Burger, B. Hackl, and W. Ring, *Incorporating topological derivatives into level set methods*, J. Comp. Phys, 194 (2004), pp. 344–362.

[6] S. Chen, B. Merriman, S. Osher, and P. Smereka, *A simple level set method for solving stefan problems*, J. Comput. Phys., 135 (1997), pp. 8–29.

[7] S. J. Cox and D. C. Dobson, *Maximizing band gaps in two-dimensional photonic crystals*, SIAM J. APPL. Math, 59 (1999), pp. 2108–2120.

[8] S. Garreau, P. Guillaume, and M. Masmoudi, *The topological asymptotic for PDE systems: The elasticity case*, SIAM J. Control Optim., 39 (2001), pp. 1756–1778.

[9] F. Gibou and R. Fedkiw, *Fast hybrid k-means level set algorithm for segmentation*, in The Procedings of the 4th Annual Hawaii International Conference on Statistics and Mathematics, 2002. Stanford Technical Report, Nov 2002.

[10] M. Hassine, S. Jan, and M. Masmoudi, *From differential calculus to 0-1 optimization*, European Congress on Computational Methods in Applied Science and Engineering, July 2004.

[11] C.-Y. Kao, S. Osher, and E. Yablonovitch, *Maximizing band gaps in two dimensional photonic crystals by using level set methods*, Applied Physics B: Lasers and Optics, 81 (2005), pp. 235–244.

[12] F. Murat and S. Simon, *Etudes de problems d'optimal design*, Lectures Notes in Computer Science, 41 (1976), pp. 54–62.

[13] A. Novotny, R. Feijoo, E. Taroco, and C. Padra, *Topological sensitivity analysis*, Comput. Methods Appl. Mech. Engrg., 192 (2003), pp. 803–829.

[14] S. Osher and F. Santosa, *Level set methods for optimization problems involving geometry and constraints*, J. Comp. Phys., 171 (2001), pp. 272–288.

[15] S. Osher and J. A. Sethian, *Fronts propagating with curvature dependent speed; algorithms based on hamilton-jacobi formulations*, J. Comput. Phys., 79 (1988), pp. 12–49.

[16] J. Sethian and A. Wiegmann, *Structural boundary design via level set method and immersed interface methods*, J. Comput. Phys., 163 (2000), pp. 489–528.

[17] J. Sokolowski and A. Zochowski, *On the topological derivative in shape optimization*, SIAM J. Control Optim., 37 (1999), pp. 1251–1272.

[18] J. Sokolowski and J.-P. Zolesio, *Introduction to Shape Optimization: Shape Sensitivity Analysis*, Springer, Heidelberg, 1992.

[19] B. Song and T. Chan, *A fast algorithm for level set based optimization*. CAM 02-68, UCLA, December 2002.

[20] H.-K. Zhao, T. Chan, B. Merriman, and S. Osher, *A variational level set approach to multiphase motion*, J. of Comput. Phys., 127 (1996), pp. 179–195.

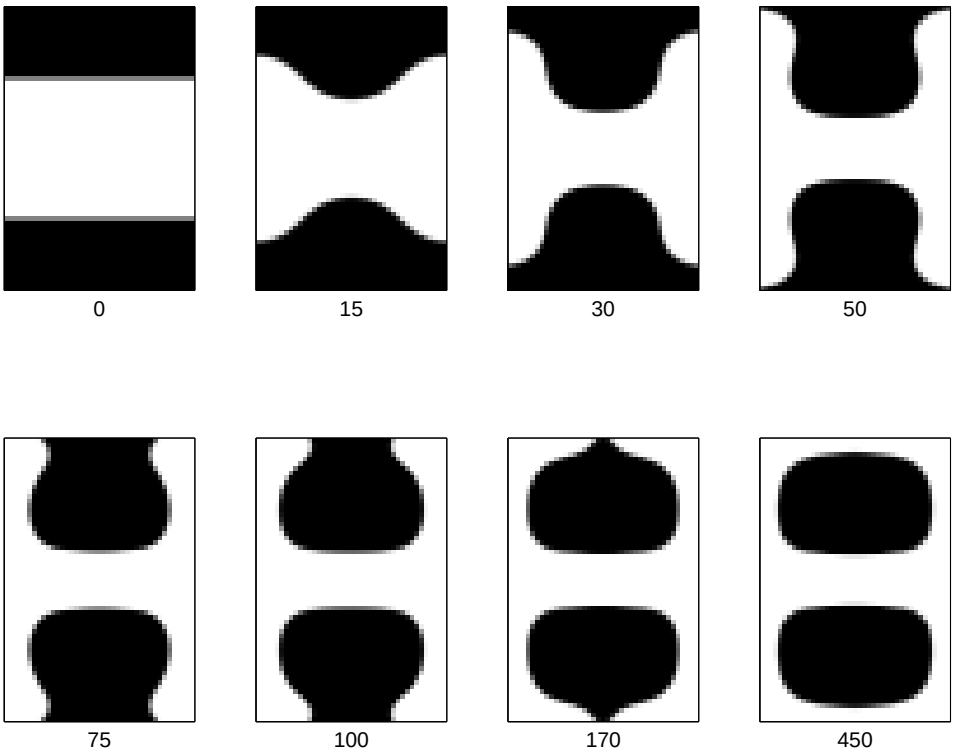

FIG. 5.6. *The evolution of the density distribution for* $\max_{\Omega} \lambda_2 - \lambda_1$ *from solving* $\phi_t + W|\nabla\phi| = 0$. *After 450 iterations,* $\max_{\Omega} \lambda_2 - \lambda_1 = 15.4618$.

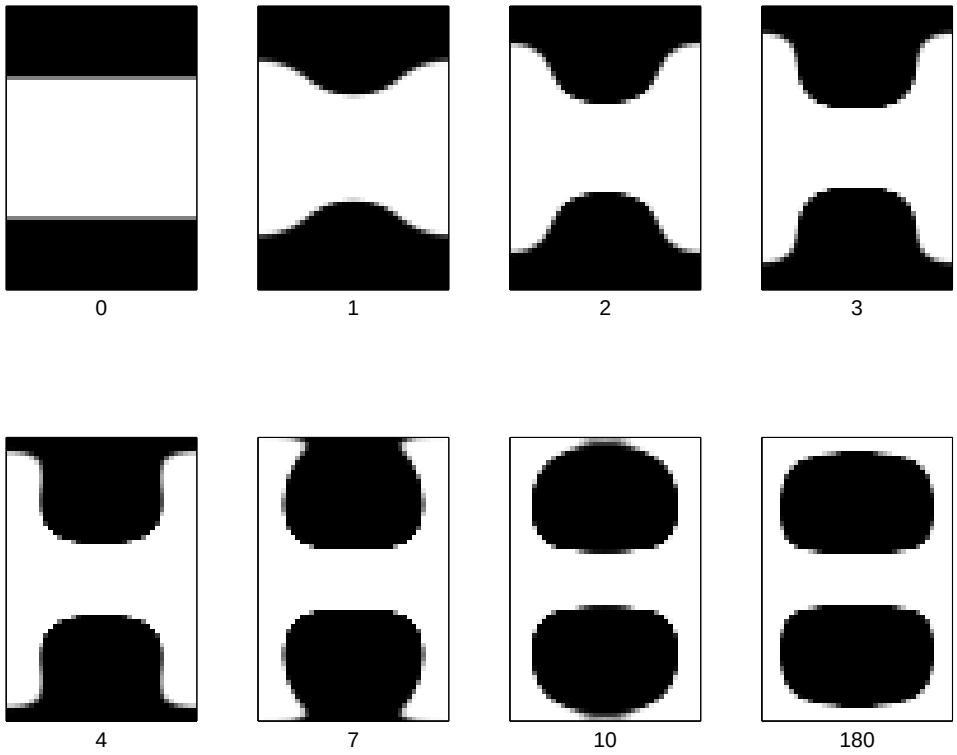

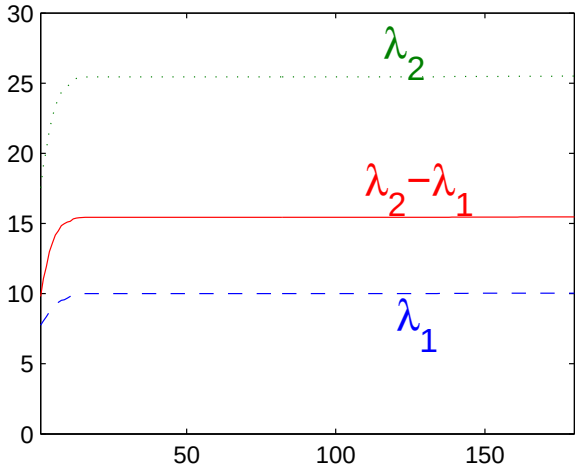

FIG. 5.7. *The evolution of the density distribution for* $\max_{\Omega} \lambda_2 - \lambda_1$ *from solving* $\phi_t + W(|\nabla\phi| + 10) = 0$. *After 180 iterations,* $\max_{\Omega} \lambda_2 - \lambda_1 = 15.4724$.

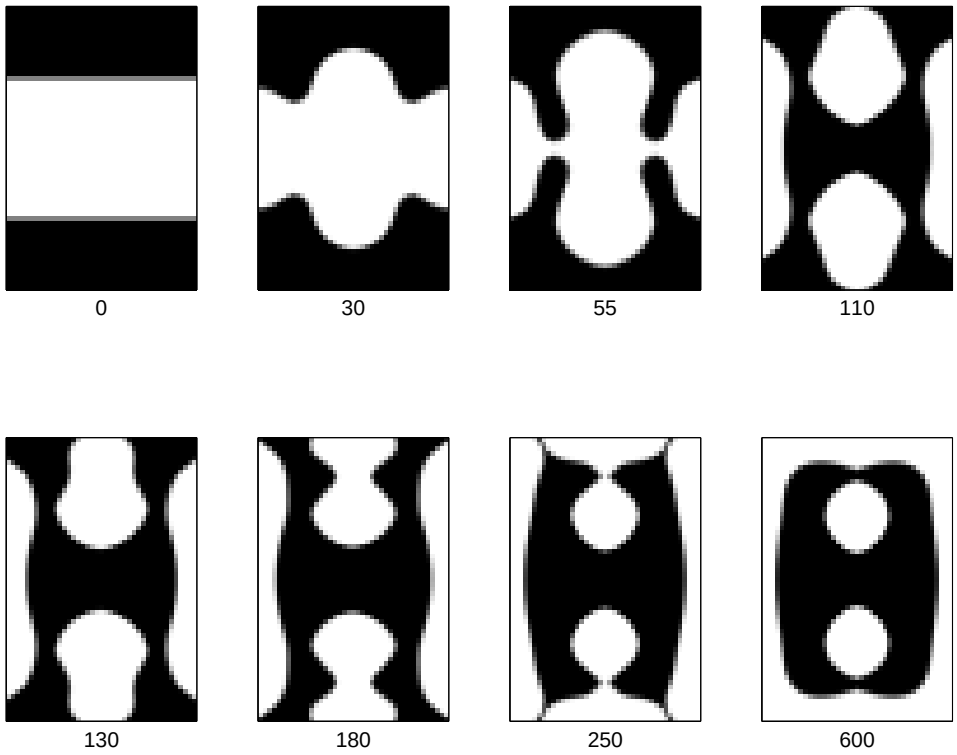

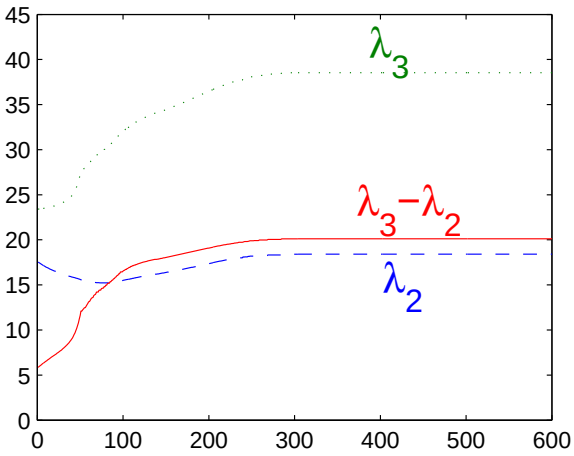

FIG. 5.8. *The evolution of the density distribution for* $\max_{\Omega} \lambda_3 - \lambda_2$ *from solving* $\phi_t + W|\nabla\phi| = 0$. *After 600 iterations,* $\max_{\Omega} \lambda_3 - \lambda_2 = 20.1239$.

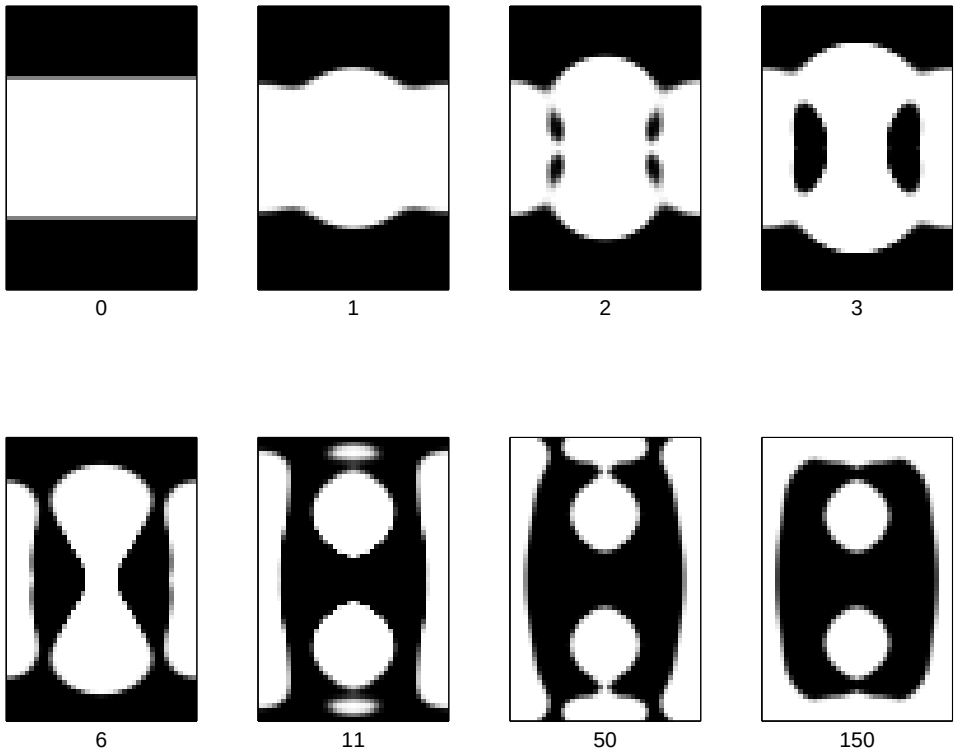

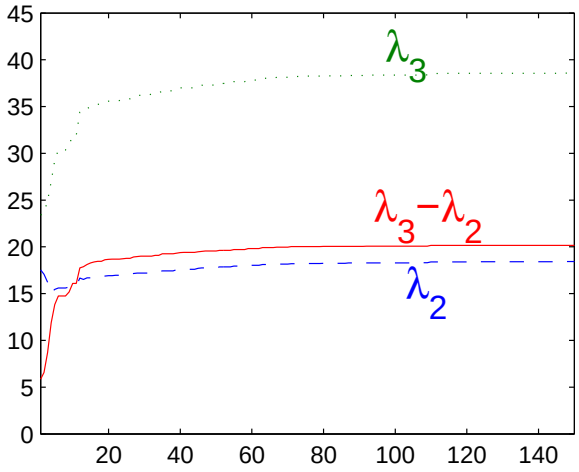

FIG. 5.9. *The evolution of the density distribution for* $\max_{\Omega} \lambda_3 - \lambda_2$ *from solving* $\phi_t + W(|\nabla\phi| + 10) = 0$. *After 150 iterations,* $\max_{\Omega} \lambda_3 - \lambda_2 = 20.1600$.

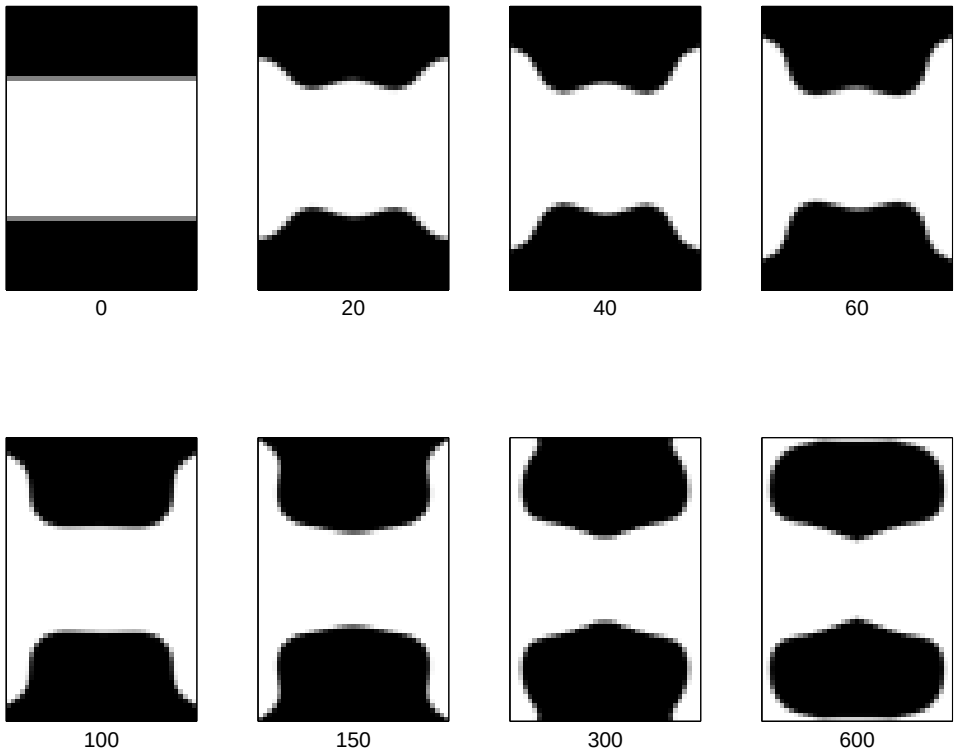

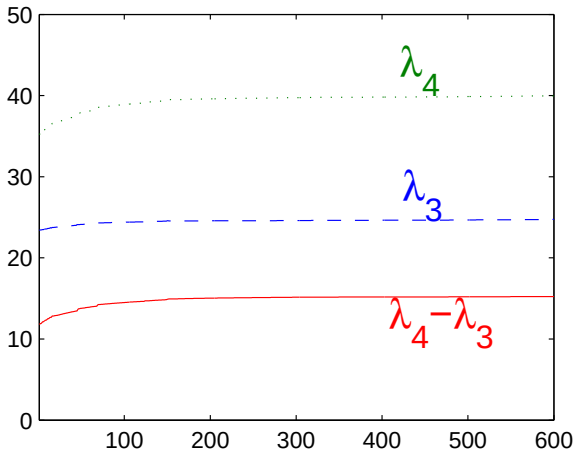

FIG. 5.10. *The evolution of the density distribution for* $\max_{\Omega} \lambda_4 - \lambda_3$ *from solving* $\phi_t + W|\nabla\phi| = 0$. *After 600 iterations,* $\max_{\Omega} \lambda_4 - \lambda_3 = 15.2323$.

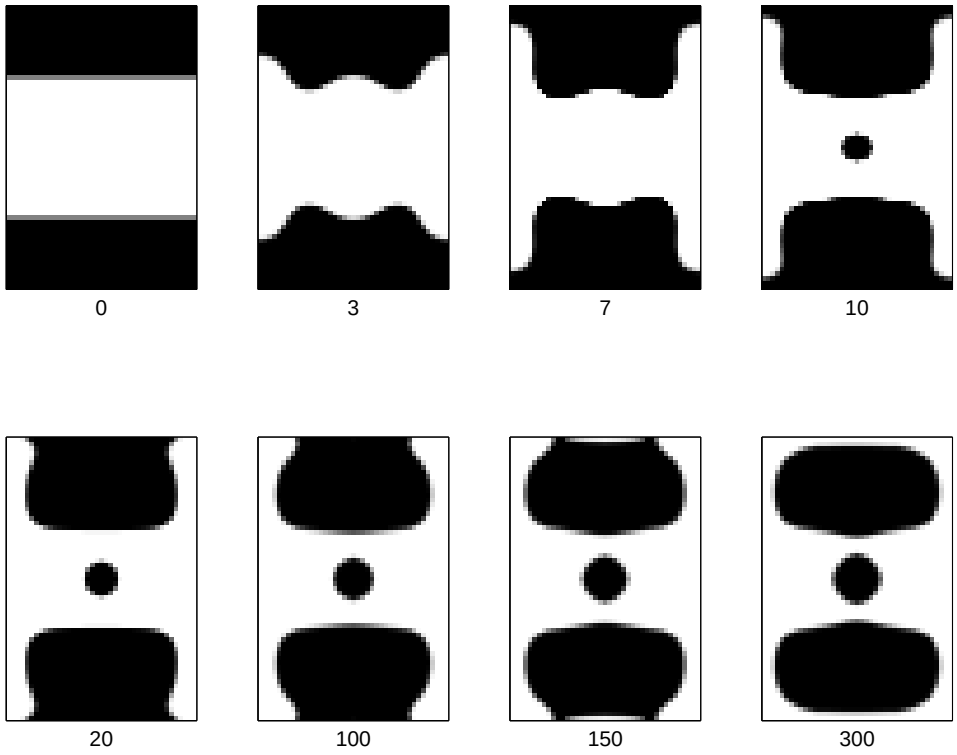

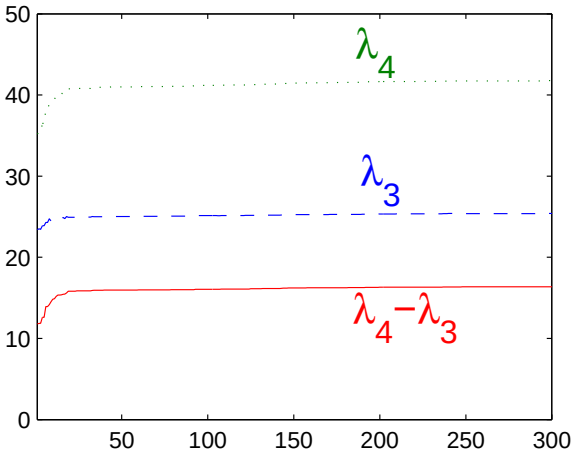

FIG. 5.11. *The evolution of the density distribution for* $\max_{\Omega} \lambda_4 - \lambda_3$ *from solving* $\phi_t + W(|\nabla\phi| + 10) = 0$. *After 300 iterations,* $\max_{\Omega} \lambda_4 - \lambda_3 = 16.3642$.

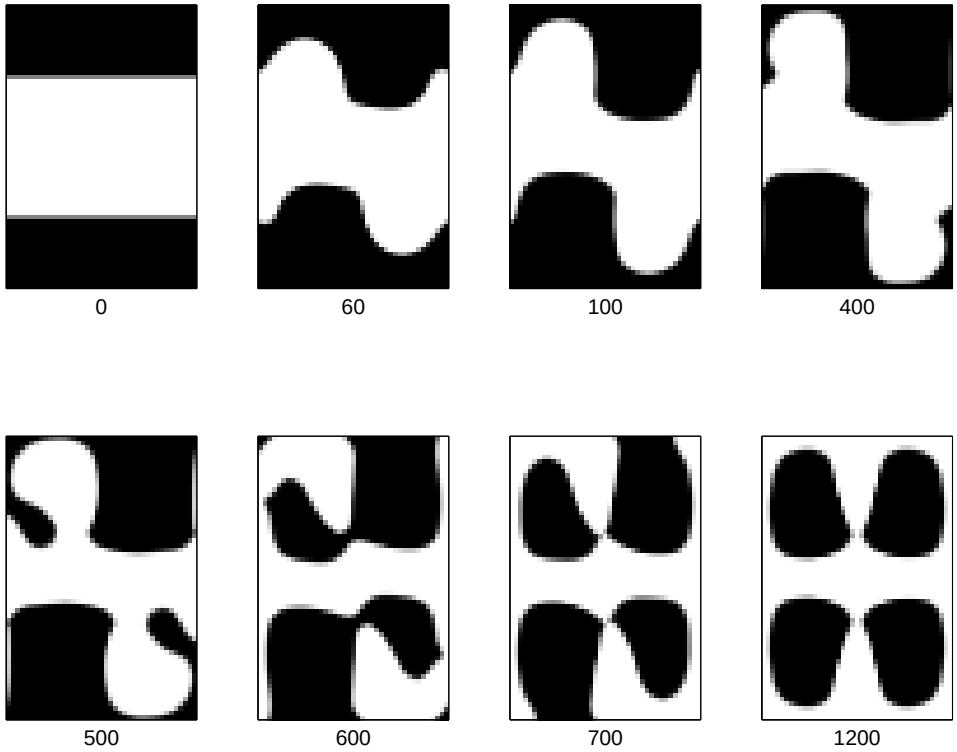

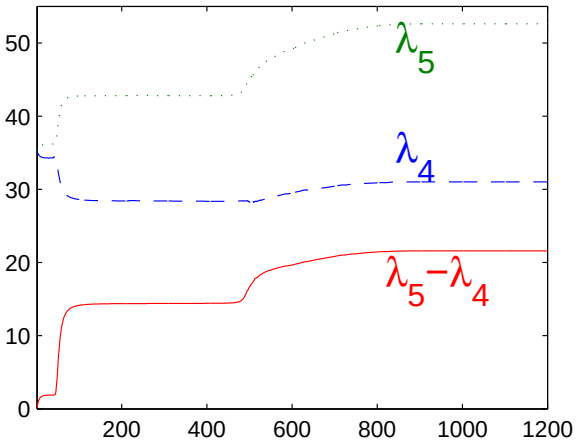

FIG. 5.12. *The evolution of the density distribution for* $\max_{\Omega} \lambda_5 - \lambda_4$ *from solving* $\phi_t + W|\nabla\phi| = 0$. *After 1200 iterations,* $\max_{\Omega} \lambda_5 - \lambda_4 = 21.5935$.

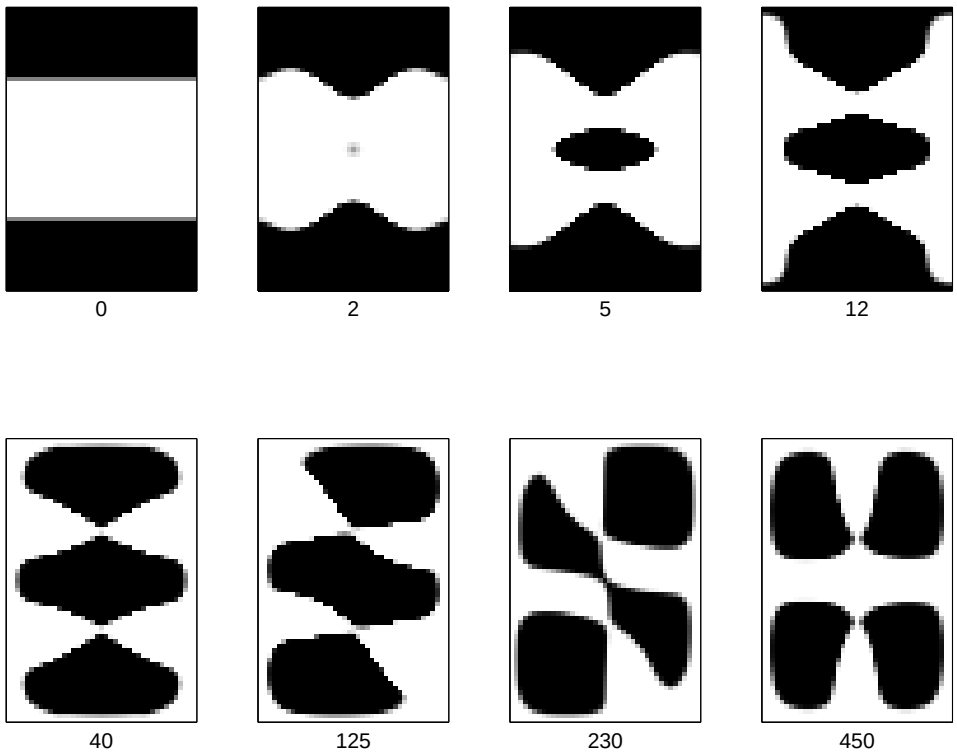

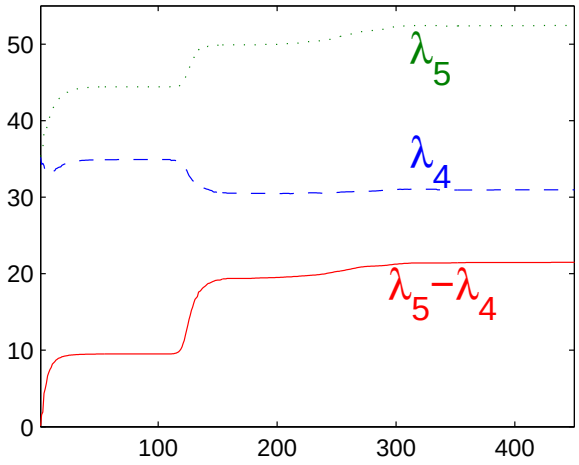

FIG. 5.13. *The evolution of the density distribution for* $\max_{\Omega} \lambda_5 - \lambda_4$ *from solving* $\phi_t + W(|\nabla\phi| + 10) = 0$. *After 450 iterations,* $\max_{\Omega} \lambda_5 - \lambda_4 = 21.4818$.

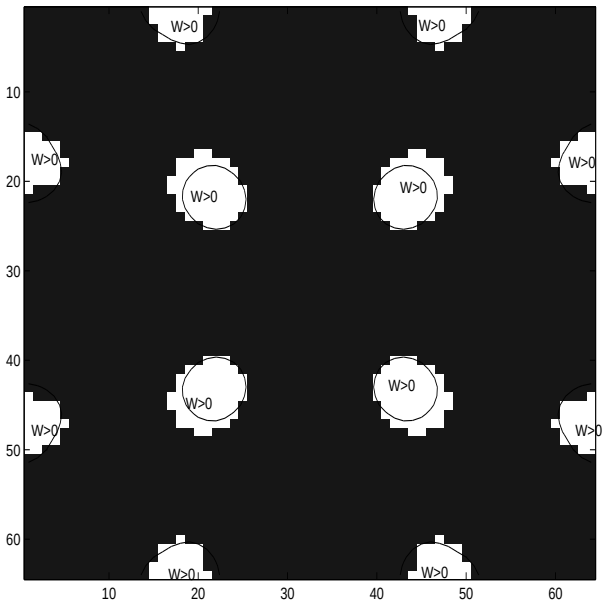

FIG. 6.1. *The "sign" picture of ϕ and W solved from $\phi_t = -W$ for maximizing the band gap between ω^8_{TM} and ω^9_{TM}. White area represents $\phi < 0$, black background represents $\phi > 0$, inside the solid circle is marked as $W > 0$ and outside the solid circle represents $W < 0$.*